






Dependence of Lévy-flight transmission on the starting point for photons propagating in atomic vapors

J. P. Lopez ¹, A. S. M. Macedo ¹, M. O. Araújo ², and T. Passerat de Silans ^{1,*}

¹*Departamento de Física, CCEN, Universidade Federal da Paraíba, Caixa Postal 5008, 58051-900 João Pessoa, Paraíba, Brazil*

²*Departamento de Física, Universidade Federal de Pernambuco, 50670-901 Recife, Pernambuco, Brazil*

 (Received 26 August 2022; revised 6 November 2022; accepted 19 December 2022; published 3 January 2023)

The propagation of a photon in an atomic medium can be seen as a Lévy-flight random walk where the probability distribution $P(z)$ for the photon step length z scales with $z^{-(\alpha+1)}$, with $0 < \alpha < 2$. In atomic vapors, previous work reported the value of α obtained from direct measurement of $P(z)$ and also from the dependence of transmission on sample opacity, both for Doppler and Lorentz profiles. In this work, we report the measurement of α in a Cs cell from the scaling of transmission with starting point, i.e., the average penetration depth of the photon in the medium before the first scattering event. We show that the parameter α depends on the size of the system and on the probability that an atom suffers a collision before spontaneous emission. The measured α parameter corresponds to the expectation value for $P(z = L)$, with L the size of the system, which is consistent with the so-called single-big-jump principle that states that a single jump rules the transport.

DOI: [10.1103/PhysRevA.107.013501](https://doi.org/10.1103/PhysRevA.107.013501)

I. INTRODUCTION

Lévy flights are a kind of particle random walk with heavy-tailed step-length distribution which favors the appearance of large steps. The step-length distribution, i.e., the probability density that a step has length z , is given asymptotically by a power law $P(z) \propto z^{-(1+\alpha)}$, with $\alpha < 2$. Although rare, those large steps dominate the particle motion, resulting in a superdiffusive displacement. Lévy flights are encountered in a large variety of systems such as displacement of cells [1], animals [2,3] and humans [4–6], economy [7,8], and, more recently, in the spread of diseases [9] and phonons transport in nanowires [10].

Photons propagating in inhomogeneous media is one of such systems where Lévy flights were evidenced. Lévy flights for photons were observed in transmission of solar light through a cloudy sky [11,12], engineered media dubbed Lévy glasses [13–15], and resonant atomic vapors [16–20]. Understanding photon transport in atomic media is important in a range of light-scattering systems, such as refined models in astrophysics [21,22]. In atomic vapors, a photon performs a random walk by means of radiation trapping, i.e., successive events of spontaneous emission of photons followed by reabsorption by the vapor. The frequency-dependent atom-photon cross section implies spectral inhomogeneity with large steps done by far-detuned emitted photons. When the photon is absorbed, the atom stays in the excited state for a typical time of a few nanoseconds before emitting a new photon, which propagates for a distance z with speed c before being reabsorbed by another atom. For vapor cell systems, whose size is of the order of cm, the travel time z/c is much smaller than the atomic lifetime τ , and Lévy flights are suitable to

describe the random walk [23]. In other applications, such as astrophysics, the travel time is not negligible and is coupled to step lengths z of the order of km, which characterizes the photon random walk as Lévy walks [23]. In both cases, the photon step-length distribution is heavy tailed and the Lévy parameter α depends on the emission and absorption spectral profiles of the vapor [24], with $\alpha = 1$ having been measured for vapor with a Doppler spectral profile [16–18] and $\alpha = 0.5$ having been measured for collisional broadened vapor exhibiting a Lorentz spectral profile [19]. Vapors subject to natural and Doppler broadenings are described by the Voigt spectral profile, which presents a Doppler core and Lorentzian wings, and these two spectral regions contribute to different step-length scales: photons emitted in the Lorentzian wings perform larger steps than those emitted in the Doppler core [20].

For bounded systems, investigation relative to the escape of the particle by one of the boundaries is a relevant problem. Indeed, depending on the system, it may not be possible to track the particle motion inside the boundaries, and measurements relative to the particles that have escaped the system through one boundary should be made. Examples of measurable quantities are the first passage time [15] and transmission [18]. For a slab geometry, the particle transmission by the boundaries depends on three parameters: the size of the system, L , the typical length scale z_{\min} , and the starting point of the random walk, z_0 . The dependence of transmission on the starting point was studied in [25] in the continuous limit for which $z_{\min} \ll z_0 \ll L$, and recently extended to all ranges of parameters [26]. Also, for finite regions, since the particle remains inside the boundaries, the Lévy random walk was predicted to converge to a normal distribution after a huge number of steps [27].

In the case of photons propagating in finite media, e.g., atomic vapors confined to cells, previous work has explored

*Corresponding author: thierry@otica.ufpb.br

the dependence of transmission on L/z_{\min} [13,18–20], which is proportional to the opacity, or optical depth, of the sample. Also, this physical system introduces a cutoff in the maximum step size of photons inside the vapor, leading to the so-called truncated Lévy flight [27]. This step-size cutoff determines the spectral region in the emission profile that contributes to the random walk inside the vapor, resulting in a size-dependent α parameter [20].

Here we explore the dependence of transmission with z_0/L for a photon in a hot vapor, contrary to the extensively studied L/z_{\min} dependence. We measure the photon transmission as the starting point z_0 in the multiple scattering regime, i.e., after the photon has undergone several scattering events before leaving the vapor. As we will show, the diffuse transmission scales with $(z_0/L)^{\alpha/2}$ [25], and we use this fact to measure the Lévy parameter α for different sample opacities. Also, we investigate the influence of atom-atom collisions in the step-length distribution and in the α parameter.

This article is organized as follows: in Sec. II, we describe the experimental setup. Then, in Sec. III, we discuss our results and compare with the theory of Lévy flight. We also discuss the possibility of investigating the dependence of transmission with z_0/L as a way to measure the parameter α . In Sec. IV, we measure the parameter α as a function of atomic density or z_{\min}/L and compare to the expectation from radiation trapping theory. Finally, we make concluding remarks in Sec. V.

II. EXPERIMENTAL SETUP

Our experimental setup is the same as in [20]. A laser beam with wavelength $\lambda = 852$ nm is incident in a sealed cell filled with cesium vapor. The coherent transmission, corresponding to photons that go through the vapor ballistically, is detected by photodetector PD1. The diffuse transmission, corresponding to photons scattered by the vapor, is detected by photodetector PD2.

The laser is a semiconductor laser with a grating external cavity emitting around the Cs D_2 line. More specifically, we scan the laser frequency around the $6S_{1/2}(F = 4) \rightarrow 6P_{3/2}(F' = 3, 4, 5)$ transitions and monitor the laser frequency with auxiliary setup including a 1.5-GHz free-spectral-range Fabry-Perot interferometer and a saturated absorption setup. The beam incident in the cell is linearly polarized, has a diameter of 1.25 mm, and its power is controlled by a $\lambda/2$ plate associated with a Glan polarizer. The incident beam power is ~ 10 μ W corresponding to $I/I_S = 0.5$, with $I_S = 1.6$ mW/cm² the saturation intensity of the corresponding transition ensuring a linear interaction between the laser and the vapor.

We use a glass cylindrical cell with radius of 1.25 cm, length of $L = 3$ cm, and a side arm containing liquid cesium. The cell and sidearm are heated by independent ovens. The cell temperature T_C regulates the vapor temperature and, consequently, the Doppler width Γ_D of the absorption profile. The side-arm temperature regulates the vapor density and is kept at least 20 °C below T_C to avoid Cs condensation on the windows. The density of the vapor is taken by fitting the coherent transmission collected on photodetector PD1 (see Fig. 1) by a Beer-Lambert law, $T_{BL} = e^{-N\sigma(x)L}$, with N the

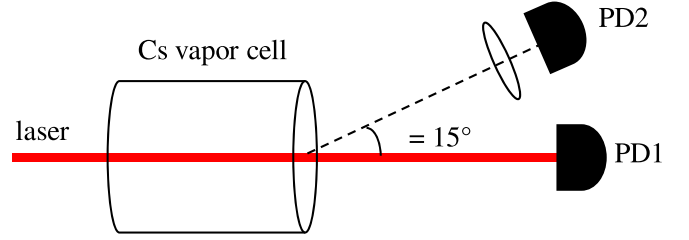


FIG. 1. Experimental setup: A low-power laser beam is incident on the vapor cell; coherent transmission and diffuse transmission are collected by photodetectors PD1 and PD2, respectively.

atomic density, x the frequency detuning, and σ the detuning-dependent photon-vapor cross section. We have varied the side-arm temperature from $T_S = 58$ °C to $T_S = 140$ °C, corresponding to vapor densities from $N = 1.5 \times 10^{11}$ atoms/cm³ to $N = 8.0 \times 10^{13}$ atoms/cm³, respectively. The interaction cross section is calculated as $\sigma(x) = \sigma_0 \sum_i \gamma_i \Phi_i(x)$, with the addition taken over the hyperfine transitions $6S_{1/2}(F = 4) \rightarrow 6P_{3/2}(F' = 3, 4, 5)$ weighted by the relative transition's strength γ_i and $\sigma_0 = \frac{3\lambda^2}{2\pi} a$. $\Phi_i(x)$ is a Voigt absorption profile centered at each hyperfine transition and normalized to $\int_{-\infty}^{\infty} dx \Phi_i(x) = 1$, given by [28]

$$\Phi_i(y) = \frac{a}{\pi^{3/2}} \int_{-\infty}^{\infty} dv \frac{e^{-v^2}}{a^2 + (y - y_i - v)^2}. \quad (1)$$

In Eq. (1), $y = x/\Gamma_D$ is a detuning normalized by Doppler width $\Gamma_D = u/\lambda$, with u the most probable thermal velocity, y_i the normalized center detuning of transition i , and Voigt parameter $a = \Gamma/2\Gamma_D$ the ratio between homogeneous and Doppler widths.

A lens before photodetector PD2 collects the photons that are scattered by the vapor in a direction with an angle θ relative to incident laser direction z . The lens has a focal length of 20 cm and is placed at 30 cm from the cell output window. Measurements are made for relatively large angle $\theta = 15^\circ$ to minimize the contribution of photons that cross the vapor ballistically and are scattered by the output window [29]. Indeed, far from resonance, photons are not scattered by the vapor and a null signal would be expected in the detector PD2. However, we observe a constant signal S_0 corresponding to photons that cross the vapor ballistically and that are scattered by the output window. Closer to resonance, such output window contribution is modulated by vapor absorption and its detuning dependence can be modeled as $S(x) = S_0 T_{BL}(x)$. The diffuse transmission T_{Diff} spectra that will be discussed in this article are obtained by subtracting the output window contribution $S(x)$ to the photodetector signal [20]. In our setup, S_0 is of the same order of magnitude as the resulting diffuse transmission T_{Diff} .

III. EXPERIMENTAL RESULTS AND DISCUSSION

A. General comments on T_{Diff} spectrum

In Fig. 2(a), we show an example of the obtained diffuse transmission (T_{Diff}) as a function of incident laser detuning. In Fig. 2, we show the diffuse transmission in red and blue lines, together with theoretical curves that will be discussed later. We plot T_{Diff} in different colors for blue and red detuning to

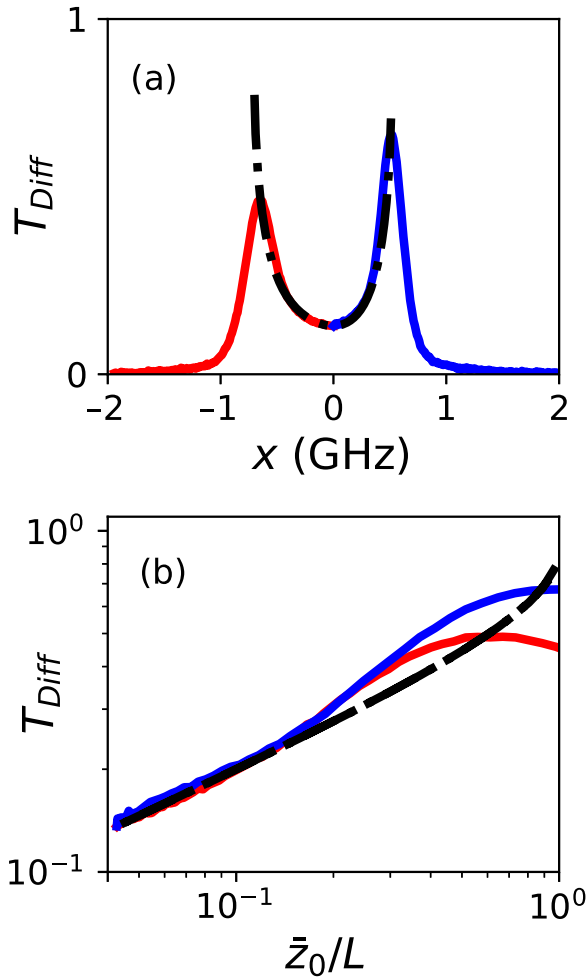


FIG. 2. Measured diffuse transmission (a) as a function of incident laser detuning and (b) as a function of \bar{z}_0/L , for a density of $N = 1.5 \times 10^{11}$ atoms/cm³ corresponding to $z_{\min}/L = 0.04$ and a Voigt parameter $a = 0.01$. Blue and red solid lines emphasize different contributions from blue- and red-detuning incident laser frequency relative to the frequency of the maximum absorption coefficient. The black dashed line corresponds to the theory of Eq. (2).

emphasize the spectrum asymmetry. From now on, detuning $x = 0$ is taken at the frequency corresponding to the maximum of the absorption coefficient, ~ 70 MHz, to the red side of the $6S_{1/2}(F = 4) \rightarrow 6P_{3/2}(F' = 5)$ transition.

Different incident photon detuning implies changing the penetration depth of the photons. With this in mind, we can transform the abscissa of Fig. 2(a) into a mean starting point of the random walk, \bar{z}_0 , by taking $\bar{z}_0 = \frac{1}{N\sigma(x)}$ as the penetration depth of the photons at detuning x . In Fig. 2(b), we plot T_{Diff} as a function of $\frac{\bar{z}_0}{L}$ in log-log scales and observe a power-law dependence in the limit $\frac{\bar{z}_0}{L} \ll 1$. A departure from the power law is observed around $\frac{\bar{z}_0}{L} \sim 10^{-1}$, with a maximum of T_{Diff} occurring around $\frac{\bar{z}_0}{L} \sim 1$ for which the photons are scattered very close to the output window.

B. Dependence of T_{Diff} on \bar{z}_0/L : Theory

Here we measure the diffuse transmission of photons through the window opposite to its incidence. The photons

perform a Lévy flight inside the vapor [16,18–20,24] with step-length distribution decaying asymptotically as $P(z) \sim 1/z^{1+\alpha}$, with α the Lévy stability parameter. The axis of the incident laser beam is denoted by z with the entrance window at $z = 0$. Three parameters are relevant in the analysis of the transmission: (i) the sample size L corresponding to the cell thickness of $L = 3$ cm; (ii) the minimum step length of the random walk, which we associate to the mean absorption length of the photon at line center $z_{\min} = \frac{1}{N\sigma(0)}$; and (iii) the starting point of the random walk $z_0 = \bar{z}_0 = \frac{1}{N\sigma(x)}$, which depends on incident photon detuning.

The case for which $z_{\min} < z_0 < L$ is known in the literature as the *continuous limit* [26] and the diffuse transmission is given by [25,30,31]

$$T_D = \left(\frac{z_0}{L}\right)^{\alpha/2} \frac{F\left(\frac{\alpha}{2}, 1 - \frac{\alpha}{2}, \frac{\alpha}{2} + 1, \frac{z_0}{L}\right)}{\frac{\alpha}{2} B\left(\frac{\alpha}{2}, \frac{\alpha}{2}\right)}, \quad (2)$$

with $F(a, b, c, d)$ the hypergeometric function and $B(a, b)$ the Euler B function.

In the limit $z_0/L \ll 1$, Eq. (2) approaches a power-law dependence [25,26,30],

$$T_D \propto \left(\frac{z_0}{L}\right)^{\alpha/2}. \quad (3)$$

Our measurements of T_{Diff} for low z_0/L are consistent with Eq. (3), exhibiting a power law. In principle, we can measure the Lévy parameter α by fitting the dependence of T_{Diff} with z_0/L by Eq. (3) and this is one of the aims of this work.

C. Diffuse transmission spectra

Before proceeding to a systematic fit of experimental curves by Eq. (3), we will discuss the whole diffuse transmission spectrum. Note that the theoretical model of Eq. (2), shown as a black dashed line in Figs. 2(a) and 2(b), does not fit well with the measured spectra for $z_0/L \sim 1$. Also, the theoretical transmission of Eq. (2) only depends on z_0/L and does not depend on whether the incident photon is blue or red detuned, as in the experimental spectrum.

a. Starting point is not well defined. For the laser incident in the vapor, the starting z_0 is not well defined. Instead, we have a probability distribution $P(z_0)dz_0$ that the incident photon is absorbed at distance between z_0 and $z_0 + dz_0$ from the entrance window,

$$P(x, z_0) = N\sigma(x)e^{-N\sigma(x)z_0}. \quad (4)$$

The diffuse transmission can now be calculated weighting Eq. (2) by $P(z_0)$,

$$T_D(x) = \int_0^L dz_0 P(x, z_0) T_D(z_0). \quad (5)$$

The diffuse transmission calculated using Eq. (5) is shown in Fig. 3(a) as a black dash-dotted line. Note that it qualitatively approaches the experimental spectra by the appearance of a maximum around $z_0/L \sim 1$. Equation (5) now takes into account that only a percentage, $1 - e^{-N\sigma L}$, of the photons is absorbed and scattered by the vapor. The maximum of T_{Diff} is a competition between the photon being scattered closer to the output window (larger z_0), thus increasing the detected signal,

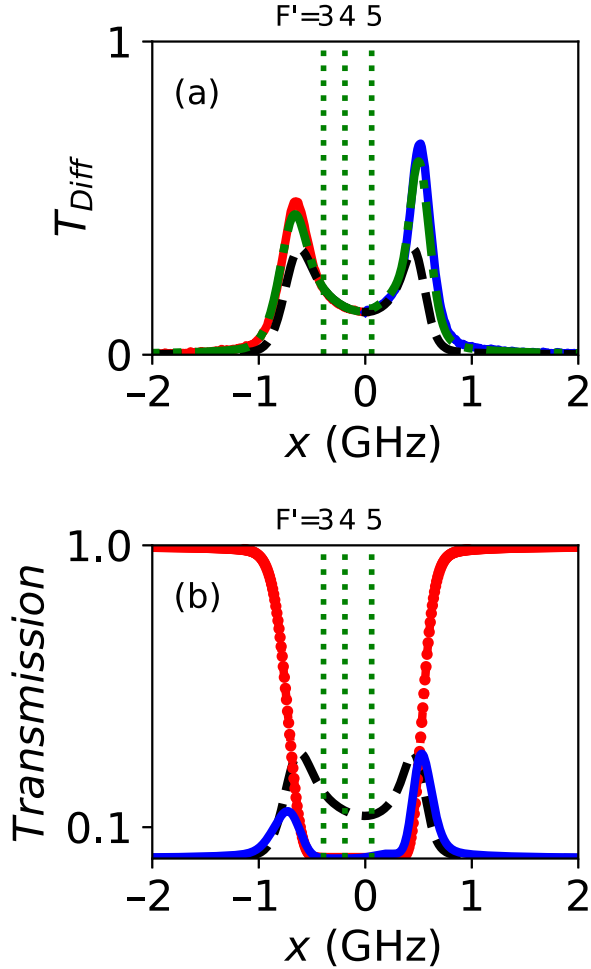


FIG. 3. (a) Measured diffuse transmission compared to the model considering one scattering contribution and multiple scattering contribution. The blue and red solid lines are the experimental diffuse transmission for incident blue and red detuning, respectively. Atomic density is $N = 1.5 \times 10^{11}$ atoms/cm³, corresponding to $z_{\min}/L = 0.04$, the same as for Fig. 2. The black dashed line is the multiple scattering contribution from Eq. (5) and the green dot-dashed line corresponds to the joint contributions of single and multiple scattering [Eq. (7)]. (b) Multiple scattering contribution to T_D from Eq. (5) (black dashed line); single scattering contribution from Eq. (8) (blue solid line) and coherent transmission (red dotted line). Vertical green dotted lines mark the positions of the hyperfine $6S_{1/2}(F = 4) \rightarrow 6P_{3/2}(F' = 3, 4, 5)$ transitions.

and a decrease of the number of photons being scattered by the vapor for large laser detuning.

For low $z_0/L \ll 1$, where the approximation of Eq. (3) is valid,

$$T_D(x) \sim \int_0^L dz_0 P(x, z_0) \left(\frac{z_0}{L}\right)^{\alpha/2} \sim \left(\frac{\bar{z}_0}{L}\right)^{\alpha/2}, \quad (6)$$

so $\bar{z}_0 = 1/N\sigma(x)$ is a good parameter for fitting experimental data to obtain α at low \bar{z}_0/L .

b. Influence of first scattering event on transmission. For a step-length distribution $P(z) = \frac{\alpha}{z_{\min}}(z_{\min}/z)^{1+\alpha}$ [32], the probability that a photon scattered at z_0 is transmitted after only one scattering scales as $\sim \frac{\alpha}{(L-z_0)^\alpha}$ and can be neglected in the

continuous limit $z_{\min} \ll \bar{z}_0 \ll L$. However, for photons propagating in resonant vapor, the step-length distribution after the first scattering is different from the subsequent scattering contributions [28,33] and the transmission contribution of this first scattering event must be considered separately. Taking into account the contribution from the first scattering event, the diffuse transmission can be written as

$$T_D(x) = T_{D,1}(x) + T_{D,M}(x), \quad (7)$$

with $T_{D,1}(x)$ the contribution of the photon escaping the cell by the output window after only one scattering event, and $T_{D,M}(x)$ the contribution of multiple scattered photons given by Eq. (5). The one scattering contribution is given by

$$T_{D,1}(x) = \int_0^L dz_0 N\sigma(x)e^{-N\sigma(x)z_0} \int_{L-z_0}^\infty dz P_1(z, x), \quad (8)$$

where $P_1(z, x)$ is the probability distribution that a photon performs a step of length z after the first scattering event that depends on incident detuning x .

The probability that a photon emitted at a given detuning x' travels a distance z before being absorbed is [34,35]

$$P(x', z) = N\sigma(x')e^{-N\sigma(x')z}. \quad (9)$$

This probability distribution of step length should be weighted by the spectral distribution of the emitted radiation field $\Theta(x', x)$,

$$P(z, x) = \int_{-\infty}^\infty dx' \Theta(x', x) N\sigma(x')e^{-N\sigma(x')z}. \quad (10)$$

In the above equation, $\Theta(x', x)$ denotes the probability that a photon is spontaneously emitted with detuning between x' and $x' + dx'$ and depends on the incident detuning x .

For a two-level atom, the emission spectrum is given by [17]

$$\Theta_1(x', x) \propto \frac{1}{4\pi^3} \int dv_1 e^{-v_1^2/u^2} \frac{1}{1 + 4(x - v_1/\lambda)^2/\Gamma^2} \times \int dv_2 e^{-v_2^2/u^2} p\left(x - v_1/\lambda, x' - \frac{\vec{v} \cdot \hat{n}'}{\lambda}\right). \quad (11)$$

In Eq. (11), $v_1(v_2)$ is the atom velocity component parallel (perpendicular) to the incoming photon direction \hat{n} , $\vec{v} = (v_1, v_2)$ is the velocity vector, $e^{-v_i^2/u^2} dv_i$ is the Maxwell-Boltzmann probability of finding an atom with velocity component between v_i and $v_i + dv_i$ in direction i , and \hat{n}' is a unit vector in the direction of the photon emission. $p(\xi', \xi)$ is the frequency redistribution function in the atomic rest frame. In the absence of collisions between atoms, the photon scattering is elastic in the atomic rest frame and $p(\xi', \xi) = \delta(\xi' - \xi)$ [21,28], while for frequent collisions, the frequency is redistributed in the atomic rest frame and $p(\xi', \xi) = \frac{\Gamma}{2\pi} \frac{1}{\Gamma^2/4 + \xi'^2}$ [21,28,36]. The total homogeneous width $\Gamma = \Gamma_n + \Gamma_C$ is the sum of natural width Γ_n and collisional broadening Γ_C . The emission spectrum in Eq. (11) is written for a two-level atom. This equation can be easily extended for the D_2 transition with three absorption transitions [$6S_{1/2}(F = 4) \rightarrow 6P_{3/2}(F' = 3, 4, 5)$, in our case] and the possibility of optical pumping to $6S_{1/2}(F = 3)$ [17].

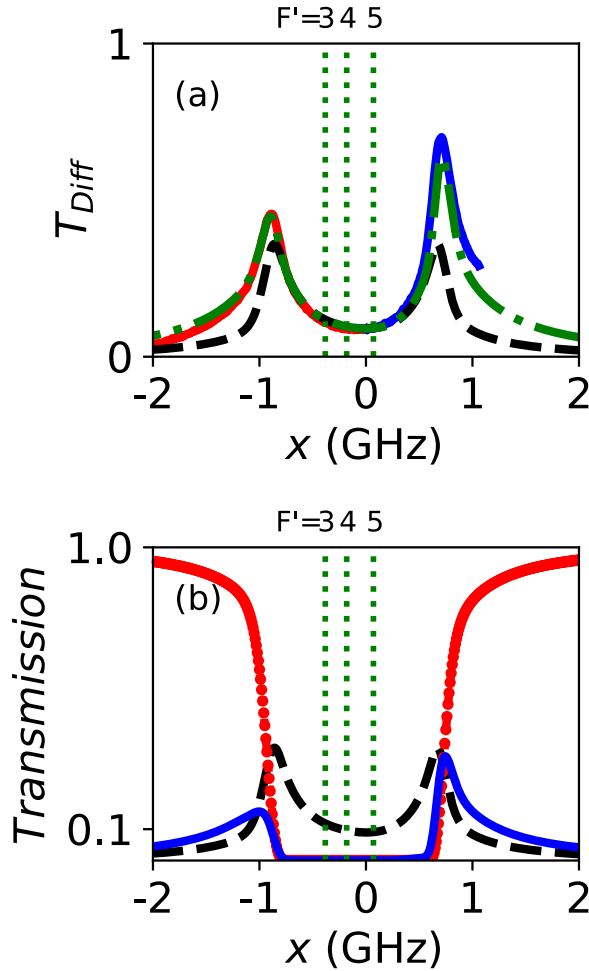


FIG. 4. (a) Measured diffuse transmission compared to the model considering one scattering contribution and multiple scattering contribution. The blue and red solid lines are the experimental diffuse transmission for incident blue and red detuning, respectively. Atomic density is $N = 2.0 \times 10^{12}$ atoms/cm³ corresponding to $z_{\min}/L = 3 \times 10^{-3}$ and a Voigt parameter $a = 0.01$. The black dashed line is the multiple scattering contribution from Eq. (5) and the green dot-dashed line corresponds to the joint contributions of single and multiple scattering [Eq. (7)]. (b) Multiple scattering contribution to T_D from Eq. (5) (black dashed line); single scattering contribution from Eq. (8) (blue dotted line) and coherent transmission (red dotted line). Vertical green dotted lines mark the positions of the hyperfine $6S_{1/2}(F = 4) \rightarrow 6P_{3/2}(F' = 3, 4, 5)$ transitions.

In Fig. 3(a), we compare the measured diffuse transmission T_{Diff} (blue and red solid lines), and theoretically obtained from Eq. (7) (green dot-dashed line) together with the contribution of multiple scattering $T_{D,M}$ [Eq. (5), black dashed line]. The calculated spectra reproduce well the measured spectrum including the maxima's positions and amplitudes. In Fig. 3(b), we compare multiple scattering $T_{D,M}$ [Eq. (5), black dashed line], single scattering (blue solid line) contributions, and coherent transmission (red dotted line). The asymmetry of the red- and blue-detuned maxima is related to one scattering contribution [blue solid line in Fig. 3(b)] and the existence of transition $6S_{1/2}(F = 4) \rightarrow 6P_{3/2}(F' = 3, 4)$ in the red side, while in the blue side, there is only one transition $6S_{1/2}(F = 4) \rightarrow 6P_{3/2}(F' = 5)$ very close to $x = 0$.

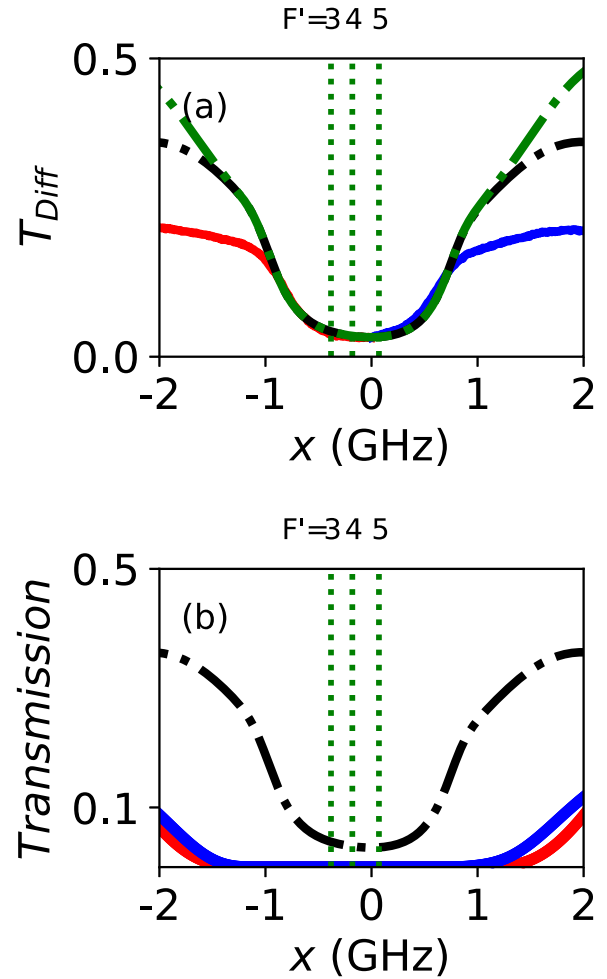


FIG. 5. (a) Measured diffuse transmission compared to the model considering one scattering contribution and multiple scattering contribution. The blue and red solid lines are the experimental diffuse transmission for incident blue and red detuning, respectively. Atomic density is $N = 6.0 \times 10^{13}$ atoms/cm³ corresponding to $z_{\min}/L = 1 \times 10^{-4}$ and a Voigt parameter $a = 0.02$. The black dashed line is the multiple scattering contribution from Eq. (5) and the green dot-dashed line corresponds to the joint contributions of single and multiple scattering [Eq. (7)]. (b) Multiple scattering contribution to T_D from Eq. (5) (black dashed line); single scattering contribution from Eq. (8) (blue dotted line) and coherent transmission (red dotted line). Vertical green dotted lines mark the positions of the hyperfine $6S_{1/2}(F = 4) \rightarrow 6P_{3/2}(F' = 3, 4, 5)$ transitions.

In Figs. 4 and 5, we show diffuse transmission and theoretical curves for higher densities. In Fig. 4, the theory of Eq. (7), considering the contribution of multiple and single scattering, reproduces the experiment well, while for higher density, in Fig. 5, the theory only fits correctly close to resonance (see Sec. III D).

D. Measurement of α parameter

One of the aims of this work is the proposal to use diffuse transmission as a function of \bar{z}_0/L to measure α in the multiple scattering regime. We note that the result of Eq. (6) is valid for $\bar{z}_0/L \ll 1$ and we will analyze the measured T_{Diff} for the

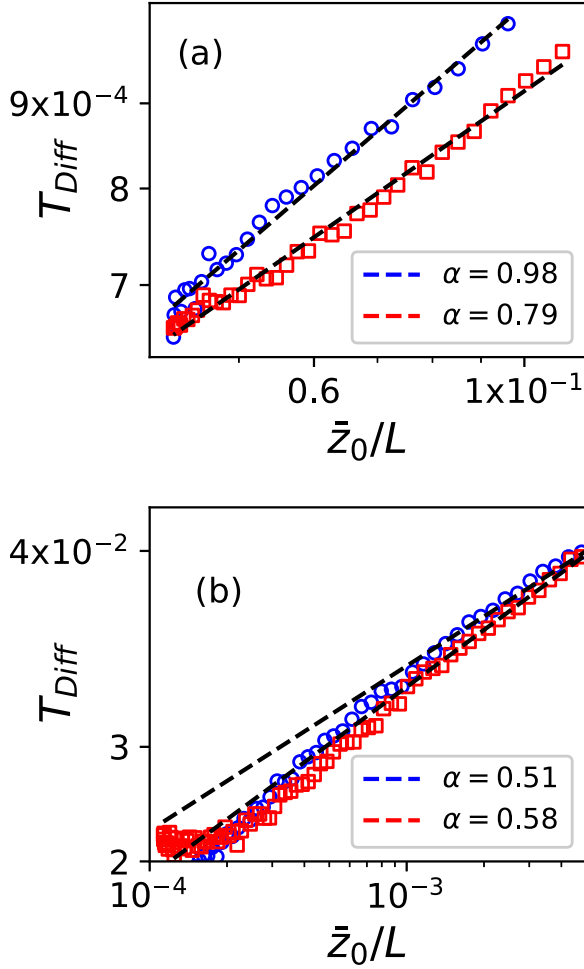


FIG. 6. Diffuse transmission as a function of \bar{z}_0/L for blue and red detuning with obtained α values from fitting Eq. (6). (a) For density $N = 1.5 \times 10^{11}$ atoms/cm³, corresponding to $z_{\min}/L = 4 \times 10^{-2}$. (b) For $N = 6.0 \times 10^{13}$ atoms/cm³, corresponding to $z_{\min}/L = 1 \times 10^{-4}$.

region $\bar{z}_0/L < 0.15$ [37]. For this region, coherent transmission is negligible (around 0.1%) and the one scattering contribution is very low [see Fig. 3(b)]. For instance, the region for which $\bar{z}_0/L < 0.15$ corresponds to the spectral range from $x = -500$ to $x = 270$ MHz for density of $N = 1.5 \times 10^{11}$ atoms/cm³ shown in Fig. 3.

Diffuse transmission as a function of \bar{z}_0/L is shown in Figs. 6(a) and 6(b), together with the obtained α values from fitting Eq. (6). For low density [Fig. 6(a) for $N = 1.5 \times 10^{11}$ atoms/cm³, corresponding to $z_{\min}/L = 4 \times 10^{-2}$], we get different power laws for blue and red side detuning with a higher value for the blue side possibly related to the nonzero contribution of one scattering [see Fig. 3(b)].

Diffuse transmission as a function of \bar{z}_0/L for high density ($N = 6.0 \times 10^{13}$ atoms/cm³, corresponding to $z_{\min}/L = 1 \times 10^{-4}$) is shown in Fig. 6(b). For higher density, a fitting range limit for incident detuning should be considered. We fit for the range $|x - x_i| < x_c$, with x_i the detuning of a hyperfine transition and the limit x_c given by [38,39]

$$\frac{e^{-x_c^2/\Gamma_D^2}}{\sqrt{\pi}} = \frac{a\Gamma_D^2}{\pi x_c^2}. \quad (12)$$

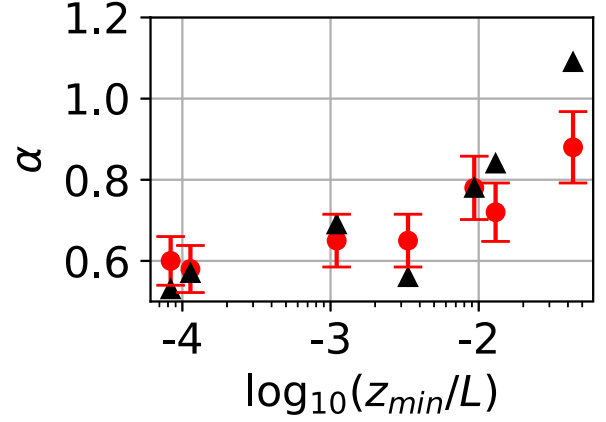


FIG. 7. Lévy parameter α measured as a function of z_{\min}/L , corresponding to different atomic densities (in red circles) and theoretical estimation (in black triangles).

For $|x - x_i| < x_c$, the photon is absorbed at the line center in the atomic rest frame and reemitted around the line center favoring frequency redistribution. For $|x - x_i| > x_c$, there exists a correlation between the incident and emitted photon frequency, resulting in step-length correlations [28,33], a situation we do not analyze here. For $a = 0.02$ [corresponding to Figs. 5 and 6(b)], we find $x_c = 2.5\Gamma_D$. As the limit between the two situations is not sharp, we take, as the limit, $|x - x_i| < 2\Gamma_D$ and thus $-1000 < x < 640$ MHz (with $\Gamma_D \approx 285$ MHz). Note that in Fig. 5(a), the region where theory does not reproduce the experiment well corresponds to $|x - x_i| > x_c$, for which correlations between successive step sizes may occur that are not considered in our analyses. Also, for densities equal to or above $N = 6.0 \times 10^{13}$ (or $z_{\min}/L < 1 \times 10^{-4}$), a departure from the power law is observed below $\bar{z}_0/L \sim 2 \times 10^{-4}$ that corresponds to very low penetration depth $\bar{z}_0 < 6 \mu\text{m}$ [see Fig. 6(b)]. These low penetration depths are of the order of the mean distance traveled by atoms during excited level lifetime $\bar{l} = u\tau \sim 7 \mu\text{m}$ and quenching of excitation may occur by collisions of excited atoms with window surface [40–42]. For the high density of Fig. 6(b), $N\lambda^3/8\pi^3 \sim 0.2$ and collective effects may deviate the absorption coefficient from the model used here. For high density, we extract α fitting Eq. (6) for $\bar{z}_0 > 30 \mu\text{m} \sim 4.3\bar{l}$ to avoid the influence of surface quenching. Note that analyzing diffuse transmission as a function of \bar{z}_0/L allows for measurement of α for each atomic density, in contrast with the previous approach of investigating transmission as a function of z_{\min}/L [18–20] for which an “averaged” α is obtained from a range of atomic densities.

The measured α parameter in the red side as a function of z_{\min}/L , corresponding to different atomic densities, is shown in Fig. 7. α depends on the ratio z_{\min}/L with $\alpha \sim 0.5$ for low z_{\min}/L (high opacities) and $\alpha \sim 1.0$ for high z_{\min}/L (low opacities) and is consistent with the expected values [20], as will be discussed in the next section. From the photodetector gain, we estimate that the detected diffuse transmission power is around 20 pW (10^{-6} of incident power) and caution must be made to eliminate spurious light from the experiment, which is the main source of uncertainty in the experiment. From repeated measurements, we estimate an uncertainty of 10% in

the measured α values. The proposed method is robust against uncertainties in parameters used to fit coherent transmission for the calculation of $\bar{z}_0 = 1/N\sigma(x)$ (see discussion in the Appendix).

IV. DISCUSSION

The theoretically expected Lévy parameter can be obtained from the step-length probability distribution given by Eq. (10). The vapor emission spectrum evolves with the number of scattering events and can be calculated as [17]

$$\Theta_{n+1}(x') = \int_{-\infty}^{\infty} \Theta_n(x) \frac{R(x', x)}{\Phi(x)} dx, \quad (13)$$

with $\Theta_n(x')$ the emission spectrum after n scattering events, $\Phi(x)$ the normalized Voigt absorption profile [Eq. (1)], and $R(x', x)$ is known as a redistribution function giving the joint probability that a photon with detuning x is absorbed and a photon with detuning x' is emitted. Expressions for $R(x', x)$ for two-level atoms and for different scenarios are given in [21,28] and can be easily extended to multiple-level atoms following Ref. [17]. We consider here the so-called R_{II} scenario corresponding to the absence of collisions between atoms and the R_{III} scenario with frequent collisions between atoms [21]. In the absence of collisions (R_{II}), the photon scattering is elastic in the atomic rest frame, resulting in partial correlations between absorbed and emitted frequency in the laboratory rest frame. We plot, in Fig. 8(a), the evolution of emission spectra in the R_{II} scenario with number of scattering events. We note that after a few scattering events ($n = 10$), the emitted spectrum $\Theta_n(x')$ evolves slowly and we consider it to have reached a stationary regime. Also in Fig. 8(a), we show a normalized Voigt absorption spectrum for two-level atoms. The Voigt absorption profile is similar to a Doppler Gaussian spectra in the core and has Lorentzian wings. For a low number of scattering events, the emission spectra $\Theta_n(x')$ approach the Doppler core of the Voigt profile. With an increasing number of scattering events, Lorentzian wings begins to appear. However, the frequency correlation in the atomic rest frames introduces a kind of cutoff in the emitted frequency [28,33] as the frequency change between consecutive scattering events is of the order of Γ_D at maximum. For calculations of the emission spectra of Fig. 8(a), we have considered the incident laser spectrum as a Dirac delta function, $\Theta_0 = \delta(x)$, since eventual photons incident in the laser spectral wings are transmitted and not scattered by the vapor [43].

For the R_{III} scenario, collisions between atoms are very frequent, randomizing the phase of atomic dipole oscillations with a mean interval τ_C between random phase changes [36,44,45]. As a consequence, there is complete frequency redistribution in the atomic rest frame with the emission spectrum following a Lorentzian with total width $\Gamma = \Gamma_n + \Gamma_C$, with $\Gamma_C = \frac{1}{2\pi\tau_C} \sim 10^{-7} \text{ Hz cm}^3 \times N$ the collisional width [46–48]. In the laboratory frame, frequency is further redistributed by the Doppler shift. We plot in Fig. 8(b) the emitted spectra Θ_n for the R_{III} scenario after n scattering events. Calculations are done using the redistribution function available in [21,28]. The emission spectrum becomes stationary after a few scattering events, reaching the complete frequency redistribution (CFR) characterized by $\Theta_n(x') = \Phi(x')$. Emission in

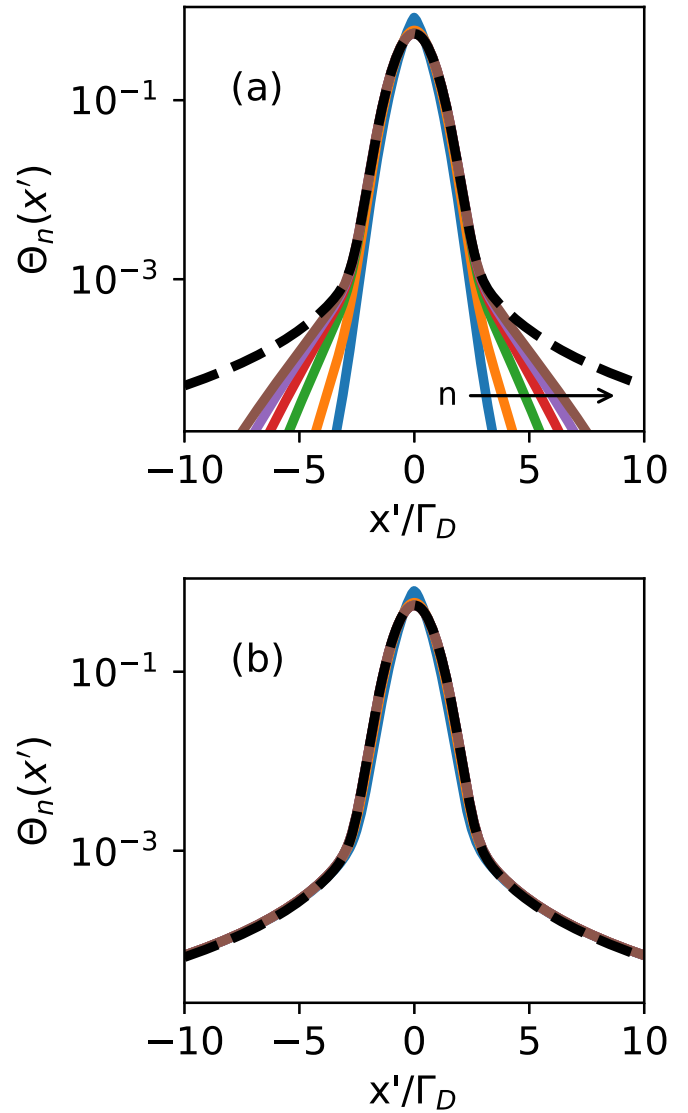


FIG. 8. Emission spectra $\Theta_n(x')$ of the vapor after n scattering events in the (a) R_{II} and (b) R_{III} scenarios for two-level atoms with Voigt parameter $a = 0.02$. Calculated spectra are for $n = 1, 2, 4, 6, 8, 10$ in both (a) and (b). The black dashed line corresponds to the Voigt absorption profile [Eq. (1)] for a two-level atom.

Lorentz wings is now present and may dominate the transport if the system is big enough to accommodate such large steps [20].

The R_{II} and R_{III} scenarios are limiting cases for which $\Gamma_C \ll \Gamma_n$ and $\Gamma_C \gg \Gamma_n$, respectively. For a general situation, the redistribution function is given by [28,38,39]

$$R(x', x) = (1 - P_C)R_{II}(x', x) + P_C R_{III}(x', x), \quad (14)$$

with branching ratio $P_C = \Gamma_C / (\Gamma_C + \Gamma_n)$. The same relation of Eq. (14) is valid for step-length distributions,

$$P(z) = (1 - P_C)P_{II}(z) + P_C P_{III}(z). \quad (15)$$

In Fig. 9, we plot $1 + \alpha$ for R_{II} (red line), R_{III} (black line), and general scenarios (blue line) obtained from step-size distributions using $1 + \alpha = -\frac{d}{d \ln(z)} \ln[P(z)]$. For the R_{III} scenario, we find the result typical for step-length distribution with Voigt

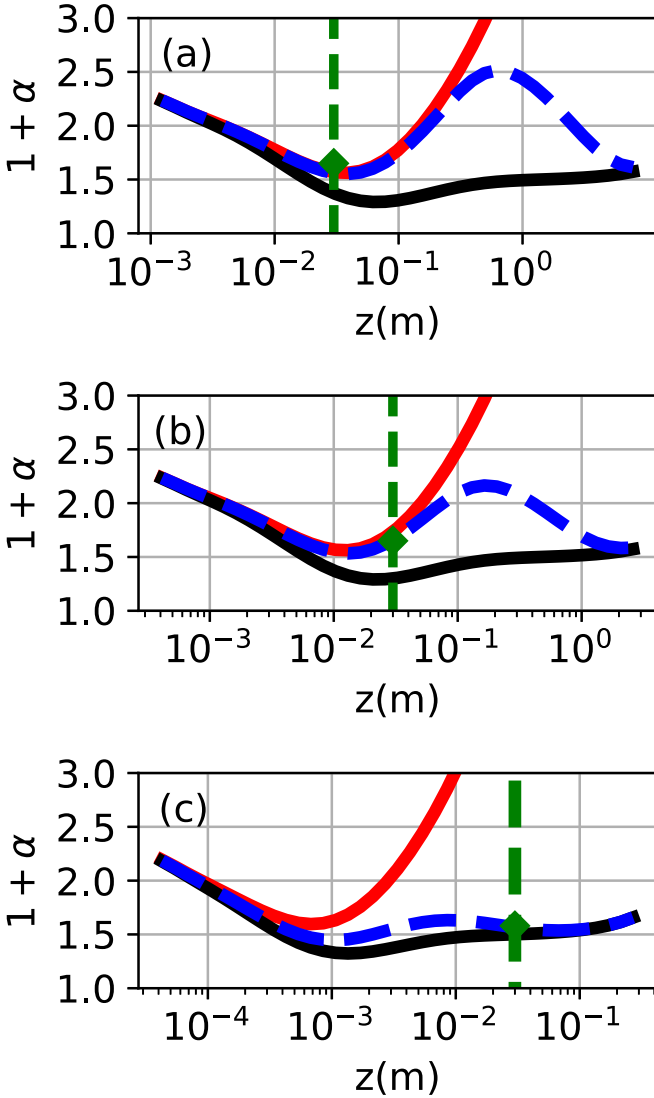


FIG. 9. Calculated $1 + \alpha = -d\ln[P(z)]/d\ln(z)$ as a function of step size z for R_{II} (red solid curve), R_{III} (black solid curve), and general (blue dashed curve) scenarios. The vertical dotted line denotes the cell length of $L = 3$ cm and the green diamond is the measured $1 + \alpha$. (a) For the atomic density of $N = 2.0 \times 10^{12}$ atoms/cm³, corresponding to $z_{\min}/L = 3 \times 10^{-3}$ and $P_C = 3 \times 10^{-2}$. (b) For the atomic density of $N = 6.0 \times 10^{12}$ atoms/cm³, corresponding to $z_{\min}/L = 1 \times 10^{-3}$ and $P_C = 10^{-1}$. (c) For the atomic density of $N = 6.0 \times 10^{13}$ atoms/cm³, corresponding to $z_{\min}/L = 1 \times 10^{-4}$ and $P_C = 5 \times 10^{-1}$.

emission and absorption profile (CFR) [34] with $\alpha \sim 1$ at small distances corresponding to a contribution of the Doppler core of the Voigt profile and $\alpha = 0.5$ for large z corresponding to a contribution of Lorentz wings [20]. For R_{II} , the emission frequency cutoff results in a step-length cutoff and an increase of the α value [28,33]. The vertical dotted line in Fig. 9 corresponds to the thickness of the sample and the triangle symbol to the measured $1 + \alpha$ from diffuse transmission. The measured $1 + \alpha$ corresponds to the value obtained from the general step-length distribution of Eq. (15) for $z = L$. This result is consistent with the *single-big-jump principle* that states that the random walk is dominated by a single big jump

and that the probability of a displacement L after a number of jumps is equal to the probability that the biggest jump has size L [49]. Theoretical α values obtained from general $P(z)$ [Eq. (15)] as a function of z_{\min}/L using the so-called single-big-jump principle are shown in Fig. 7 in black triangles and are consistent with the measured values. We stress that for each theoretical point of Fig. 7, we have used experimental parameters (density and Voigt parameters) extracted from fitting of the coherent transmission to calculate $P(z)$ and thus extract the α values. Note that in principle, the emitted spectrum $\Theta_n(x')$ depends on the incident detuning, but for the detuning range analyzed, $|x - x_i| < x_c = 2\Gamma_D$, the frequency is redistributed around the line center after a few scattering events [33]. We have checked that calculating step-size distributions for $|x - x_i| = x_c$ changes the expected α value by only 5%. Collisions between atoms are necessary for emission in Lorentzian wings [see Fig. 8(b)] and measurement of $\alpha \sim 0.5$ as evidenced in Fig. 9(c) for $\Gamma_C \sim \Gamma_n$. Collisional contribution could influence the random walk even for $\Gamma_C \ll \Gamma_n$ [Figs. 9(a) and 9(b)] provided the system is large, a situation encountered in astrophysical systems [22].

Equation (3) used to model the scaling of diffuse transmission with z_0/L was deduced for a one-dimensional Lévy flight or a three-dimensional slab geometry, whereas our cell is cylindrical with a radius smaller than the thickness ($R < L$). For a cylindrical cell, we can write $T'_D = T_D[1 - T_L(r = R)]$, with $T_L(r = R)$ the probability that the photons escapes by the cell lateral surface. From the random walk point of view, $T_L(r = R)$ does not depend on z_0 . Furthermore, $T_L(r = R)$ does not depend on the incident frequency as long as the incident laser is close to resonance: the emission spectrum in the transverse direction is centered at $x' = 0$ and independent of incident detuning for $x < 2.5\Gamma_D$ [38]. We conclude that the scaling law of Eq. (3) is still valid for the cylindrical cell used.

V. CONCLUSIONS

In conclusion, we have investigated the transmission of photons through a hot atomic vapor in the regime of multiple scattering. We have shown that the transmission spectra can be interpreted using the physics of random walk. We have confirmed the scalability of the transmission with starting point of the random walk [25,26,30] and measured the Lévy-flight parameter α . The starting point of the random walk was changed by sweeping the incident laser frequency around the D_2 line, thus modifying the penetration depth in the sample. This allows one to measure α for a given atomic density, in contrast with the previous method [18–20] that measured an “averaged” value for a density range. Measurement of α for a given density permits a better understanding of the influence of collisions between atoms for the superdiffusion. In [18,19], the Lévy parameter α was also measured for a given atomic density from the radial profile of diffuse transmission. However, such method requires cell thickness that is much smaller than the diameter ($L \ll R$), a constraint that is not present in the proposed method that can be used with cells with larger L values. We give evidence that collisions are needed for emission on the Lorentz wings of the Voigt profile, the spectral region responsible for the larger steps [20,28], resulting in $\alpha \sim 0.5$. In summary, the α parameter for photons in atomic

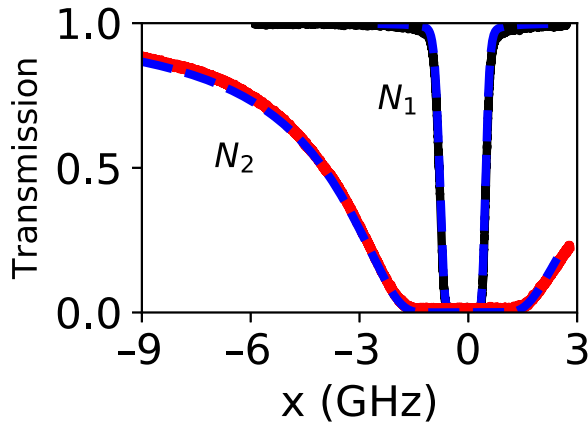


FIG. 10. Examples of measured coherent transmissions (solid lines) with fits (dashed lines) used to extract the atomic density. $N_1 = 1.5 \times 10^{11}$ atoms/cm³ and $N_2 = 6.0 \times 10^{13}$ atoms/cm³.

vapor depends both on system size (z_{\min}/L) and on the probability of collisions between atoms. Theoretical estimations [see Figs. 9(a) and 9(b), for instance] suggest that collisions may play an important role in photon transport, even for dilute vapor ($\Gamma_C \ll \Gamma_n$), provided the system is large enough. This can be important for the investigation of photon transport in astrophysical samples. The measured α corresponds to the expected value for a step of length $z = L$, which is consistent with the single-big-jump principle [49].

We have observed a deviation of the experimental data from power law $(\bar{z}_0/L)^{\alpha/2}$ for very small \bar{z}_0 (for $\bar{z}_0 < 10 \mu\text{m}$). Further investigation will be needed to understand this result. As already discussed, a hypothesis is that it may be due to collisions between excited atoms and the input cell surface [42]. Also, for high densities, it is known that atom-atom collisions, frequency shifts, and even cooperative effects such as the cooperative Lamb shift take place [50], impacting the estimation of the absorption coefficient.

ACKNOWLEDGMENTS

The authors acknowledge financial support from Coordenação de Aperfeiçoamento de Pessoal de Nível Superior (CAPES), Conselho Nacional de Desenvolvimento Científico e Tecnológico (CNPq), and Paraíba State Research Foundation (Pronex/Fapesq-PB/CNPq and Grant No. 2021/3218). This work was funded by the Public Call No. 03 Produtividade em Pesquisa PROPESQ/PRPG/UFPB Grant No. PVA13235-2020.

APPENDIX

One important point of the proposed method is to extract the detuning-dependent absorption coefficient from coherent transmission to be able to plot diffuse transmission as a function of \bar{z}_0/L . In this Appendix, we discuss the robustness of the technique for extracting the Lévy parameter α from the scaling of diffuse transmission with \bar{z}_0/L .

First of all, we plot in Fig. 10 two examples of coherent transmission together with fits using the procedure discussed in Sec. II of the main text.

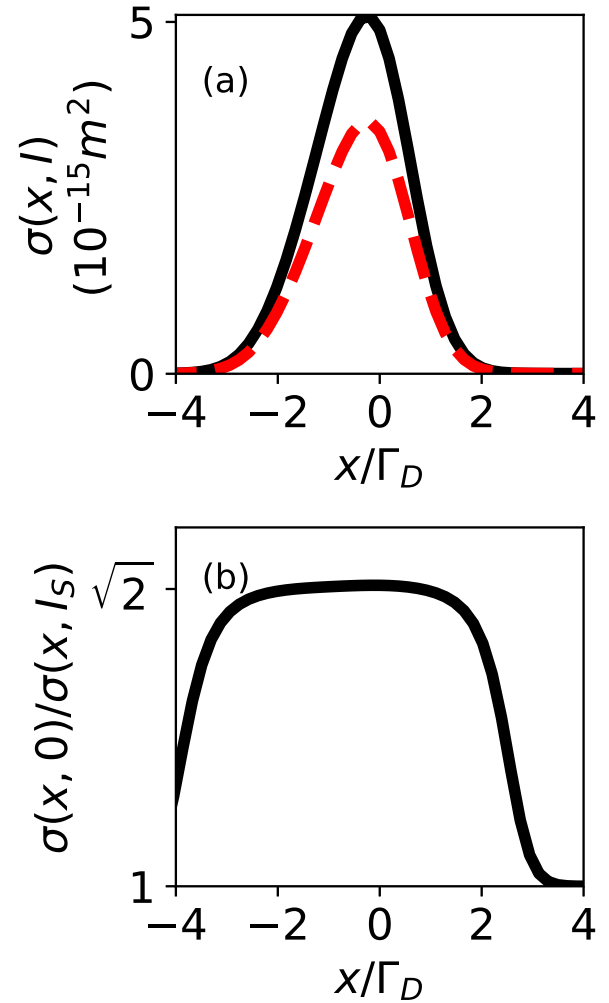


FIG. 11. (a) Calculated cross section for $I = 0$ [$\sigma(x, 0)$, black solid line] and for $I = I_S$ [$\sigma(x, I_S)$, red dashed line] for $N = 2.0 \times 10^{12}$ atoms/cm² and $\Gamma_C = 0.03\Gamma_n$. (b) Ratio between the two calculated cross sections.

Although the fits are not perfect, we argue that extracting the Lévy parameters is robust against the relevant parameters' uncertainty.

The starting point of the random walk is calculated as $\bar{z}_0 = \frac{1}{N\sigma(x)}$. So the scaling law can be written as $(\bar{z}_0/L)^{\alpha/2} = \frac{1}{N^{\alpha/2}} (\frac{1}{\sigma(x)L})^{\alpha/2}$. The density enters as a multiplying factor and does not influence the α determination.

Voigt profiles are characterized by parameter $a = \Gamma/2\Gamma_D$ that depends both on the Doppler width, related to cell temperature, and on the homogeneous width $\Gamma = \Gamma_n + \Gamma_C$, which depends on the collisional width. For the range of densities used in the experiment, $\Gamma \ll \Gamma_D$ and the cross section should not change significantly with Γ_C uncertainty in the spectral range $-3.2\Gamma_D < x < 2\Gamma_D$ used for obtaining α . Indeed, we have calculated $\sigma(x)$ for one of the measurement conditions [$N = 2.0 \times 10^{12}$ atoms/cm², $\Gamma_C = 0.03\Gamma_n$, corresponding to Figs. 4 and 9(a)] and also for an increased value of $\Gamma_C = \Gamma_n$. The change in calculated $\sigma(x)$ for $\Gamma_C = \Gamma_n$ was of 10% at maximum. A similar result was obtained when we calculated $\sigma(x)$ for an increased temperature of the cell of $T_C = 170^\circ\text{C}$ instead of the actual value of $T_C = 160^\circ\text{C}$. This is expected

since the Doppler width varies slowly with cell temperature, as $\sqrt{T_C}$.

Another parameter that may influence the $\sigma(x)$ calculation is the laser intensity. As $I = 0.5I_S$, we have used $I = 0$ in our calculations. To compare, we have calculated $\sigma(x)$ for $I = I_S$. The calculated $\sigma(x)$ for $I = 0$ and $I = I_S$ are shown

in Fig. 11(a) for comparison, together with the ratio between the two $\sigma(x)$ in Fig. 11(b). In the Doppler core, it is expected that saturation diminishes the cross section by an almost constant factor $\sqrt{1 + I/I_S}$, which is confirmed in Fig. 11(b). The maximum change of $\sigma(x)$ for $I = I_S$ for the spectral range of $-3.2\Gamma_D < x < 2\Gamma_D$ is of 5%.

-
- [1] S. Huda, B. Weigelin, K. Wolf, K. V. Tretiakov, K. Polev, G. Wilk1, M. Iwasa, F. S. Emami, J. W. Narojczyk, M. Banaszak, S. Soh, D. Pilans, A. Vahid, M. Makurath, P. Friedl, G. G. Borisy, K. Kandere-Grzybowska, and B. A. Grzybowski, Lévy-like movement patterns of metastatic cancer cells revealed in microfabricated systems and implicated *in vivo*, *Nat. Commun.* **9**, 4539 (2018).
- [2] G. M. Viswanathan, V. Afanasyev, S. V. Buldyrev, E. J. Murphyt, P. Princet, and H. E. Stanley, Lévy flight search patterns of wandering albatrosses, *Nature (London)* **381**, 413 (1996).
- [3] B. Ríos-Uzeda, E. Brigatti, and M. V. Vieira, Lévy like patterns in the small-scale movements of marsupials in an unfamiliar and risky environment, *Sci. Rep.* **9**, 2737 (2019).
- [4] D. Brockmann, L. Hufnagel, and T. Geisel, The scaling laws of human travel, *Nature (London)* **439**, 462 (2006).
- [5] M. C. González, C. A. Hidalgo, and A.-L. Barabási, Understanding individual human mobility patterns, *Nature (London)* **453**, 779 (2008).
- [6] A. Reynolds, E. Ceccon, C. Baldauf, T. K. Medeiros, and O. Miramontes, Lévy foraging patterns of rural humans, *PLoS One* **13**, e0199099 (2018).
- [7] B. Podobnik, A. Valentiničič, D. Horvatić, and H. E., Asymmetric Lévy flight in financial ratios, *Proc. Natl. Acad. Sci. USA* **108**, 17883 (2011).
- [8] S. C. Lera and D. Sornette, Gross domestic product growth rates as confined Lévy flights: Towards a unifying theory of economic growth rate fluctuations, *Phys. Rev. E* **97**, 012150 (2018).
- [9] C. J. Tessone, M. Cencini, and A. Torcini, Synchronization of Extended Chaotic Systems with Long-Range Interactions: An Analogy to Lévy-Flight Spreading of Epidemics, *Phys. Rev. Lett.* **97**, 224101 (2006).
- [10] J. Li, L. Weng, J. Xie, J. Amrit, and A. Ramiere, Lévy walk of quasiballistic phonons in nanowires, *Phys. Rev. E* **105**, 064123 (2022).
- [11] M. M. Novak and T. G. Dewey, *Fractal Frontiers: Fractals In The Natural And Applied Sciences* (World Scientific, Singapore, 1997).
- [12] K. Pfeilsticker, F. Erle, O. Funk, H. Veitel, and U. Platt, First geometrical pathlengths probability density function derivation of the skylight from spectroscopically highly resolving oxygen a-band observations: 1. Measurement technique, atmospheric observations and model calculations, *J. Geophys. Res. Atmos.* **103**, 11483 (1998).
- [13] P. Barthelemy, J. Bertolotti, and D. S. Wiersma, A Lévy flight for light, *Nature (London)* **453**, 495 (2008).
- [14] P. Barthelemy, J. Bertolotti, K. Vynck, S. Lepri, and D. S. Wiersma, Role of quenching on superdiffusive transport in two-dimensional random media, *Phys. Rev. E* **82**, 011101 (2010).
- [15] R. Savo, M. Burresti, T. Svensson, K. Vynck, and D. S. Wiersma, Walk dimension for light in complex disordered media, *Phys. Rev. A* **90**, 023839 (2014).
- [16] N. Mercadier, W. Guerin, M. Chevrollier, and R. Kaiser, Lévy flights of photons in hot atomic vapours, *Nat. Phys.* **5**, 602 (2009).
- [17] N. Mercadier, M. Chevrollier, W. Guerin, and R. Kaiser, Microscopic characterization of Lévy flights of light in atomic vapors, *Phys. Rev. A* **87**, 063837 (2013).
- [18] Q. Baudouin, R. Pierrat, A. Eloy, E. J. Nunes-Pereira, P.-A. Cuniasse, N. Mercadier, and R. Kaiser, Signatures of Lévy flights with annealed disorder, *Phys. Rev. E* **90**, 052114 (2014).
- [19] M. O. Araújo, T. P. de Silans, and R. Kaiser, Lévy flights of photons with infinite mean free path, *Phys. Rev. E* **103**, L010101 (2021).
- [20] A. S. M. Macedo, J. P. Lopez, and T. Passerat de Silans, Sample size effects for Lévy flight of photons in atomic vapors, *Phys. Rev. E* **104**, 054143 (2021).
- [21] D. G. Hummer, Non-coherent scattering: I. The redistribution function with Doppler broadening, *Mon. Not. R. Astron. Soc.* **125**, 21 (1962).
- [22] D. G. Hummer, Non-coherent scattering—III: The effect of continuous absorption on the formation of spectral lines, *Mon. Not. R. Astron. Soc.* **138**, 73 (1968).
- [23] V. Zaburdaev, S. Denisov, and J. Klafter, Lévy walks, *Rev. Mod. Phys.* **87**, 483 (2015).
- [24] E. Pereira, J. M. G. Martinho, and M. N. Berberan-Santos, Photon Trajectories in Incoherent Atomic Radiation Trapping as Lévy Flights, *Phys. Rev. Lett.* **93**, 120201 (2004).
- [25] S. V. Buldyrev, S. Havlin, A. Y. Kazakov, M. G. E. da Luz, E. P. Raposo, H. E. Stanley, and G. M. Viswanathan, Average time spent by Lévy flights and walks on an interval with absorbing boundaries, *Phys. Rev. E* **64**, 041108 (2001).
- [26] J. Klinger, R. Voituriez, and O. Bénichou, Splitting Probabilities of Symmetric Jump Processes, *Phys. Rev. Lett.* **129**, 140603 (2022).
- [27] R. N. Mantegna and H. E. Stanley, Stochastic Process with Ultraslow Convergence to a Gaussian: The Truncated Lévy Flight, *Phys. Rev. Lett.* **73**, 2946 (1994).
- [28] A. R. Alves-Pereira, E. J. Nunes-Pereira, J. M. G. Martinho, and M. N. Berberan-Santos, Photonic superdiffusive motion in resonance line radiation trapping partial frequency redistribution effects, *J. Chem. Phys.* **126**, 154505 (2007).
- [29] In [19], simulations indicate that diffuse transmission is independent of measurement angle, results reinforced by [20] that have obtained by angle-independent measured α values.
- [30] S. Buldyrev, M. Gitterman, S. Havlin, A. Kazakov, M. da Luz, E. Raposo, H. Stanley, and G. Viswanathan, Properties of Lévy flights on an interval with absorbing boundaries, *Physica A* **302**, 148 (2001).

- [31] N. S. Nicolau, H. A. Araújo, G. M. Viswanathan, M. G. E. da Luz, and E. P. Raposo, Mean first passage time and absorption probabilities of a Lévy flier on a finite interval: Discrete space and continuous limit via Fock space approach, *J. Phys. A: Math. Theor.* **54**, 325006 (2021).
- [32] C. W. Groth, A. R. Akhmerov, and C. W. J. Beenakker, Transmission probability through a Lévy glass and comparison with a Lévy walk, *Phys. Rev. E* **85**, 021138 (2012).
- [33] João Carlos de A. Carvalho, M. Oriá, M. Chevrollier, Hugo L. D. de Souza Cavalcante, and T. Passerat de Silans, Redistribution of light frequency by multiple scattering in a resonant atomic vapor, *Phys. Rev. A* **91**, 053846 (2015).
- [34] M. Chevrollier, Radiation trapping and Lévy flights in atomic vapours: An introductory review, *Contemp. Phys.* **53**, 227 (2012).
- [35] T. Holstein, Imprisonment of resonance radiation in gases, *Phys. Rev.* **72**, 1212 (1947).
- [36] E. L. Lewis, Collisional relaxation of atomic excited states, line broadening and interatomic interactions, *Phys. Rep.* **58**, 1 (1980).
- [37] This choice is a compromise between respecting the condition $\bar{z}_0 \ll L$ and having enough T_{diff} variation in the desired region to fit a power law.
- [38] H. A. Post, Radiative transport at the 184.9-nm Hg resonance line. I. Experiment and theory, *Phys. Rev. A* **33**, 2003 (1986).
- [39] F. Vermeersch, V. Fiermans, J. Ongena, H. A. Post, and W. Wieme, Monte Carlo investigation of imprisonment of resonance radiation with partial frequency redistribution, *J. Phys. B: At., Mol. Opt. Phys.* **21**, 1933 (1988).
- [40] A. G. Zajonc and A. V. Phelps, Nonradiative transport of atomic excitation in Na vapor, *Phys. Rev. A* **23**, 2479 (1981).
- [41] H. van Kampen, V. A. Sautenkov, A. M. Shalagin, E. R. Eliel, and J. P. Woerdman, Dipole-dipole collision-induced transport of resonance excitation in a high-density atomic vapor, *Phys. Rev. A* **56**, 3569 (1997).
- [42] J. C. de Aquino Carvalho and T. Passerat de Silans, Backward fluorescence of optically thick Cs vapor: Experiment and Monte Carlo simulations, *J. Quantum Spectrosc. Radiat. Transfer* **260**, 107469 (2021).
- [43] The calculated $\Theta_{n,II}(x')$ in [17] exhibits no cutoff in the Lorentzian wings since they have considered a Lorentzian laser spectrum and infinite vapor.
- [44] N. Allard and J. Kielkopf, The effect of neutral nonresonant collisions on atomic spectral lines, *Rev. Mod. Phys.* **54**, 1103 (1982).
- [45] W. J. Alford, N. Andersen, K. Burnett, and J. Cooper, Collisional redistribution of light: Far-wing line shapes and polarizations for the Ba-(Ar,Xe) systems, *Phys. Rev. A* **30**, 2366 (1984).
- [46] A. M. Akulshin, V. L. Velichanskii, A. S. Zibrov, V. V. Nikitin, V. V. Sautenkov, E. K. Iurkin, and N. V. Senkov, Collisional broadening of intra-Doppler resonances of selective reflection on the D₂ line of cesium, *JETP Lett.* **36**, 303 (1982).
- [47] Z. Jabbour, J. Sagle, R. Namiotka, and J. Huennekens, Measurement of the self-broadening rate coefficients of the cesium resonance lines, *J. Quantum Spectrosc. Radiat. Transfer* **54**, 767 (1995).
- [48] T. P. de Silans, Determination of atomic density and collisional broadening of an alkali vapor by resonant interferometry, *J. Phys. B: At., Mol. Opt. Phys.* **51**, 195401 (2018).
- [49] A. Vezzani, E. Barkai, and R. Burioni, Single-big-jump principle in physical modeling, *Phys. Rev. E* **100**, 012108 (2019).
- [50] T. Peyrot, Y. R. P. Sortais, A. Browaeys, A. Sargsyan, D. Sarkisyan, J. Keaveney, I. G. Hughes, and C. S. Adams, Collective Lamb Shift of a Nanoscale Atomic Vapor Layer within a Sapphire Cavity, *Phys. Rev. Lett.* **120**, 243401 (2018).